

RSC Advances

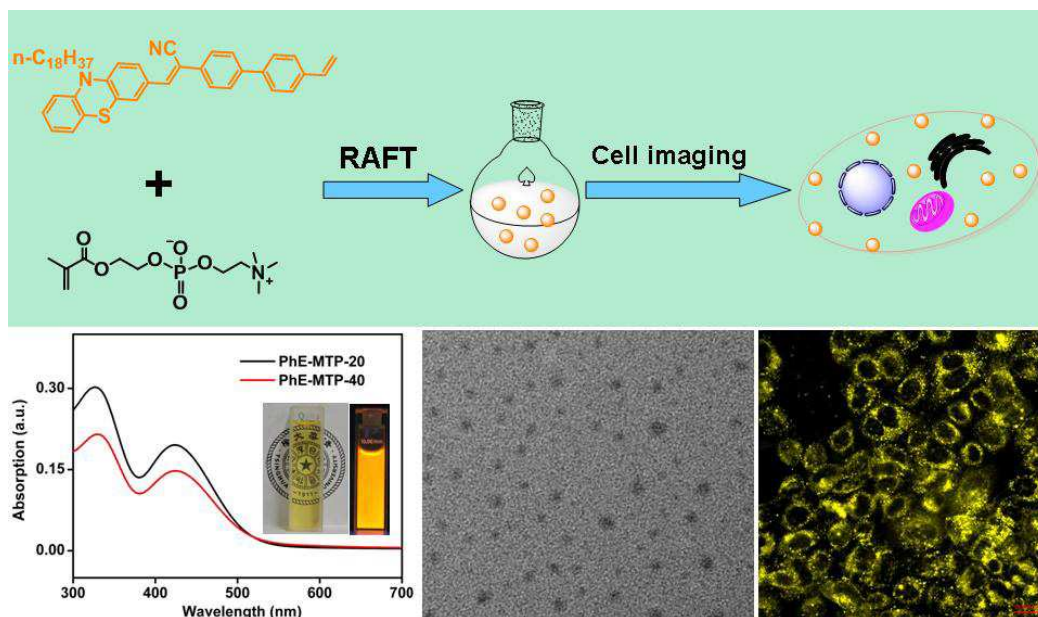


This is an *Accepted Manuscript*, which has been through the Royal Society of Chemistry peer review process and has been accepted for publication.

Accepted Manuscripts are published online shortly after acceptance, before technical editing, formatting and proof reading. Using this free service, authors can make their results available to the community, in citable form, before we publish the edited article. This *Accepted Manuscript* will be replaced by the edited, formatted and paginated article as soon as this is available.

You can find more information about *Accepted Manuscripts* in the [Information for Authors](#).

Please note that technical editing may introduce minor changes to the text and/or graphics, which may alter content. The journal's standard [Terms & Conditions](#) and the [Ethical guidelines](#) still apply. In no event shall the Royal Society of Chemistry be held responsible for any errors or omissions in this *Accepted Manuscript* or any consequences arising from the use of any information it contains.



Ultrabright and biocompatible luminescent polymeric nanoparticles were prepared via RAFT polymerization of an AIE dye and a zwitterionic monomer.

Cite this: DOI: 10.1039/c0xx00000x

www.rsc.org/xxxxxx

Full Paper

Ultrabright and Biocompatible AIE Dye Based Zwitterionic Polymeric Nanoparticles for Biological Imaging

Meiying Liu^a, Xiqi Zhang^b, Bin Yang^b, Fengjie Deng^a, Zengfang Huang^{b,c}, Yang Yang^b, Zhen Li^b, Xiaoyong Zhang^{a,b,*}, Yen Wei^{b,*}

Received (in XXX, XXX) Xth XXXXXXXXX 20XX, Accepted Xth XXXXXXXXX 20XX
DOI: 10.1039/b000000x

The development of novel fluorescent nanoprobe with remarkable optical properties, suitable particle size, high water dispersibility and good biocompatibility has recently attracted increasing interest for various biomedical applications. In this work, a novel type of luminescent polymeric nanoparticles based on polymerizable dyes with aggregation induced emission (AIE) properties and a zwitterionic monomer were prepared via reversible addition fragmentation chain transfer polymerization. Due to their amphiphilic properties, these copolymers could readily self-assemble into AIE dye contained luminescent zwitterionic polymeric nanoparticles, which were characterized by a series of characterization techniques including transmission electronic microscopy, Fourier transform infrared spectroscopy, fluorescence spectroscopy and X-ray photoelectron spectroscopy. Results showed that these luminescent polymeric nanoparticles with diameter at tens of nanometers showed high water dispersibility and strong fluorescence in aqueous solution. To explore their potential for biomedical applications, biocompatibility and cell uptake behavior of these luminescent polymeric nanoparticles were further evaluated. We demonstrated that these polymeric nanoparticles are biocompatible with A549 cells and promising for bioimaging applications. Taken advantage of these merits of AIE dye based zwitterionic polymeric nanoparticles, which could elegantly avoid the aggregation induced quenching of conventional organic dyes and nonbiodegradability of fluorescent inorganic nanoparticles, these ultrabright and biocompatible luminescent polymeric nanoparticles described in this work should be of highly potential for various biomedical applications.

1. Introduction

Over the past few decades, there is an increasing current interest for fabrication of novel fluorescent nanoprobe owing to their superior luminescent properties and multifunctional capability as compared with conventional organic dyes.¹ A promising nanoprobe should be of remarkable luminescent properties, good biocompatibility, high water stability and suitable particle size.²⁻⁹ Although a number of fluorescent nanoprobe based on inorganic, organic and hybrid components have thus been developed since the first reports of using semiconductor quantum dots for biomedical applications.¹⁰⁻¹³ Most of currently used nanoprobe are still difficult to fulfill the requirement for biomedical applications due to their inherent limitations. For example, the fluorescent inorganic nanoparticles such as semiconductor quantum dots with tunable luminescent properties, controllable morphology and high photostability are promising for bioimaging applications, however, their accumulation in reticuloendothelial system (RES) and verified toxicity of semiconductor quantum dots from heavy metal compositions made their biomedical applications still under intensive debate.^{14, 15}

To overcome the inherent shortcoming of fluorescent inorganic nanoparticles, fluorescent organic nanoparticles have recently emerged as alternative candidates for biomedical applications due to their relative better biocompatible and biodegradability.¹⁶⁻²⁸ To date, various

luminescent polymeric nanoparticles based on conventional organic dyes, conjugated polymers, aggregation induced emission (AIE) dyes and polydopamine have been reported.²⁹⁻³⁴ A general strategy for preparation of fluorescent organic nanoparticles is incorporation of hydrophobic organic dyes into amphiphilic copolymers, which can be self-assembled into core-shell polymeric nanoparticles in aqueous solution through hydrophobic interactions.³⁵ Upon self-assembly, the hydrophobic dyes were encapsulated in the core of nanoparticles, while the hydrophilic segments were expanded into water, endowing them water dispersibility. However, it is still challengeable to obtain fluorescent organic nanoprobe with strong luminescent intensity due to the notorious aggregation-caused quenching (ACQ) effect of most organic dyes.³⁶ Therefore, development of novel fluorescent polymeric nanoparticles which could overcome the ACQ effect of conventional organic dyes is of great research interest.

AIE is an abnormal optical phenomenon, which suggested some organic dyes could emitted much stronger fluorescence in their solid or aggregated state than in solution.³⁷⁻⁴³ Taken advantage of the unique AIE properties, luminescent polymeric nanoparticles based on AIE dyes could therefore elegantly avoid the ACQ effect of conventional organic dyes, which provided an novel approach to develop ultrabright and biodegradable luminescent polymeric nanoparticles.⁴⁴ In recent years, a number of dyes with AIE properties were

synthesized and various strategies for fabrication of AIE dye based luminescent nanoparticles were developed.⁴⁵⁻⁵⁶ These novel luminescent nanoparticles has demonstrated to be very promising for biomedical applications for their superior luminescent properties, good biocompatibility, biodegradable potential.

Zwitterionic polymers are a very important class of functional polymers which simultaneously contained both cationic and anionic functional groups in polymer pendant-side chains. Due to their unique molecular structures, excellent chemical properties, hydration capacity, and preferable thermal stability, zwitterionic polymers have attracted a great deal of research interest in recent years.⁵⁷ Various zwitterionic polymers have been synthesized and explored for various applications in the fields such as petroleum industry, sewage treatment, drug synthesis and biomedical applications. Especially, due to their special anti-polyelectrolyte behavior in solution, zwitterionic polymers are expected more suitable for fabrication of zwitterionic polymers contained copolymers for biomedical applications.

In this contribution, a biocompatible zwitterionic monomer 2-methacryloyloxyethyl phosphorylcholine (named as MTP) was copolymerized with a polymerizable AIE dye (named as PhE) through reversible addition fragmentation chain transfer (RAFT) polymerization. Due to their amphiphilic properties, thus obtained copolymers could self-assemble into core-shell nanoparticles (named as **PhE-MTP** NPs) which exhibited strong fluorescence and high water dispersibility in aqueous solution. To explore their bioimaging applications, biocompatibility and cell uptake behavior of thus obtained zwitterionic polymeric nanoparticles were further evaluated.

2. Experimental details

2.1 Materials and measurements

All of the chemical agents and solvents were obtained from commercial sources and used as received. PhE was synthesized and characterized in our previous report.²⁰ UV-visible absorption spectra were recorded on UV/Vis/NIR Perkin-Elmer lambda750 spectrometer (Waltham, MA, USA) using quartz cuvettes of 1 cm path length. Fluorescence spectra were measured on a PE LS-55 spectrometer with a slit width of 3 nm for both excitation and emission. On the other hand, fluorescence stability of **PhE-MTP** NPs in aqueous solution was also recorded on a PE LS-55 spectrometer under time drive model. The excitation wavelength was set at 488 nm with slit width of 15 nm and the emission wavelength was set at 581 nm with slit width of 10 nm. The fluorescence quantum yields (Φ_F) of **PhE-MTP** NPs in aqueous solution were measured using Rhodamine 6G in ethanol as the standard ($\Phi_F = 95\%$), the absorbance of the solutions was kept around 0.05 to avoid internal filter effect.⁵⁸ The X-ray photoelectron spectra (XPS) were performed on a VGESCALAB 220-IXL spectrometer using an Al K α X-ray source (1486.6 eV). The energy scale was internally calibrated by referencing to the binding energy (Eb) of the C1s peak of a carbon contaminant at 284.6 eV. The Fourier transform infrared spectroscopy (FT-IR) spectra were obtained in a transmission mode on a Perkin-Elmer Spectrum 100

spectrometer (Waltham, MA, USA). Typically, 8 scans at a resolution of 1 cm⁻¹ were accumulated to obtain one spectrum.

Transmission electron microscopy (TEM) images were recorded on a JEM-1200EX microscope operated at 100 kV, the TEM specimens were made by placing a drop of the nanoparticles suspension on a carbon-coated copper grid. The size distribution of **PhE-MTP** NPs in water was determined using a zeta Plus apparatus (ZetaPlus, Brookhaven Instruments, Holtsville, NY). ¹H NMR spectra were measured on a JEOL 400 MHz spectrometer [d₆-DMSO as solvent and tetramethylsilane (TMS) as the internal standard]. Gel permeation chromatography (GPC) analyses of polymers were performed using DMF as the eluent. The GPC system was a Shimadzu LC-20AD pump system comprising of an auto injector, a MZ-Gel SD plus 10.0 mm guard column (50×8.0 mm, 10² Å) followed by a MZ-Gel SD plus 5.0 μm bead-size columns (50-10⁶ Å, linear) and a Shimadzu RID-10A refractive index detector. The system was calibrated with narrow molecular weight distribution polystyrene standards ranging from 200 to 10⁶ gmol⁻¹.

1.2 Preparation of PhE-MTP NPs

CTA (9.7 mg, 0.037 mmol), PhE (50 mg, 0.074 mmol), MTP (200 mg, 0.67 mmol), AIBN (3.0 mg) and DMF (5 mL) were introduced in schlenk tube and purged by nitrogen flow for 30 min. The above mixture was put into an oil bath maintained at 70 °C for 12 h. Then stopped the reaction of polymerization, and dialyzed against tap water for 24 h and ethanol for 6 h using 7000 Da Mw cutoff dialysis membranes. Finally, the solution in dialysis bag was carried out by freeze-drying to obtain **PhE-MTP-20** NPs. For synthesis of **PhE-MTP-40** NPs, CTA was changed to 4.85 mg.

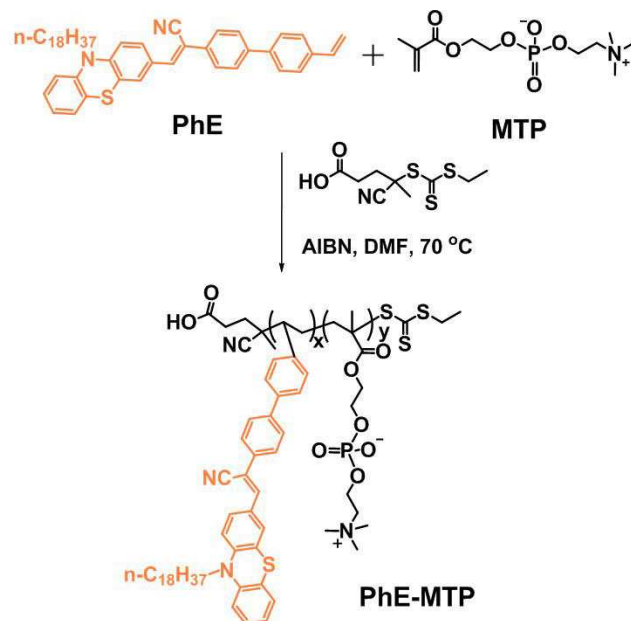


Fig. 1 Synthesis of **PhE** based luminescent polymeric nanoparticles via RAFT polymerization.

1.3 Cytotoxicity of PhE-MTP NPs

Cell morphology observation was to examine the effects of **PhE-MTP** NPs to A549 cells.^{59, 60} Briefly, cells were seeded

in 6-well microplates at a density of 1×10^5 cells mL^{-1} in 2 mL of respective media containing 10% fetal bovine serum (FBS). After cell attachment, plates were washed with PBS and cells were treated with complete cell culture medium, or different concentrations of **PhE-MTP** NPs prepared in 10% FBS containing media for 24 h. Then all samples were washed with PBS three times to remove the uninternalized nanoparticles. The morphology of cells was observed by using an optical microscopy (Leica, Germany), the overall magnification was $\times 100$.

The cell viability of **PhE-MTP** NPs on A549 cells was evaluated by cell counting kit-8 (CCK-8) assay based on our previous reports.^{61, 62} Briefly, cells were seeded in 96-well microplates at a density of 5×10^4 cells mL^{-1} in 160 μL of respective media containing 10% FBS. After 24 h of cell attachment, the cells were incubated with 10, 20, 40, 80, 120 $\mu\text{g mL}^{-1}$ **PhE-MTP** NPs for 8 and 24 h. Then nanoparticles were removed and cells were washed with PBS three times. 10 μL of CCK-8 dye and 100 μL of DMEM cell culture medium were added to each well and incubated for 2 h at 37 °C. Plates were then analyzed with a microplate reader (VictorIII, Perkin-Elmer). Measurements of formazan dye absorbance were carried out at 450 nm, with the reference wavelength at 620 nm. The values were proportional to the number of live cells. The percent reduction of CCK-8 dye was compared to controls (cells not exposure to **PhE-MTP** NPs), which represented 100% CCK-8 reduction. Three replicate wells were used per microplate, and the experiment was repeated three times. Cell survival was expressed as absorbance relative to that of untreated controls. Results are presented as mean \pm standard deviation (SD).

1.4 Confocal microscopic imaging of cells using **PhE-MTP** NPs

A549 cells were cultured in Dulbecco's modified eagle medium (DMEM) supplemented with 10% heat-inactivated FBS, 2 mM glutamine, 100 U mL^{-1} penicillin, and 100 $\mu\text{g mL}^{-1}$ of streptomycin. Cell culture was maintained at 37 °C in a humidified condition of 95% air and 5% CO_2 in culture medium. Culture medium was changed every three days for maintaining the exponential growth of the cells. On the day prior to treatment, cells were seeded in a glass bottom dish with a density of 1×10^5 cells per dish. On the day of treatment, the cells were incubated with **PhE-MTP** NPs at a final concentration of 10 $\mu\text{g mL}^{-1}$ for 3 h at 37 °C. Afterward, the cells were washed three times with PBS to remove the **PhE-MTP** NPs and then fixed with 4% paraformaldehyde for 10 min at room temperature. Cell images were taken with a confocal laser scanning microscope (CLSM) Zesis 710 3-channel (Zesis, Germany) with the excitation wavelength of 543 nm.

3. Results and discussion

3.1 Characterization of **PhE-MTP** NPs

Thus obtained **PhE-MTP** NPs were first characterized by ^1H NMR spectra (Fig. S1). Many characteristic signals of PhE and MTP were observed through ^1H NMR spectra, implying the successful copolymerization of PhE and MTP. The

number average molecular weight (M_n) of **PhE-MTP** was also determined by GPC, which showed that the M_n values of **PhE-MTP-20** and **PhE-MTP-40** are 41900 and 79800 Da with narrow polydispersity index (PDI = 1.16 and 1.19 for **PhE-MTP-20** and **PhE-MTP-40**), respectively (Fig. S2). The GPC results further confirmed successful synthesis of **PhE-MTP**. Due to the amphiphilic properties of **PhE-MTP**, which could self-assemble in aqueous solution. As evidenced by TEM images, many spherical nanoparticles with diameter at tens of nanometers were observed (Fig. 2). No significant difference was found between the diameter of **PhE-MTP-20** NPs (Fig. 2A) and **PhE-MTP-40** NPs (Fig. 2B). Furthermore, the hydrodynamic size of **PhE-MTP** NPs was also determined by dynamic light scattering (DLS). Results showed that the size distribution of **PhE-MTP-20** NPs and **PhE-MTP-40** NPs in water is 132.4 ± 58.9 and 136.3 ± 59.5 nm, respectively (Fig. S3). As compared the hydrodynamic size of **PhE-MTP** NPs, the size of **PhE-MTP** NPs characterized by TEM is somewhat smaller, which might be due to the shrinkage of micelle for TEM observation. As compared with our previous reports, the size of **PhE-MTP** NPs is relative small.^{63, 64} The possible reason may be ascribed to the unique zwitterionic properties of MTP, which could given better water dispersibility.

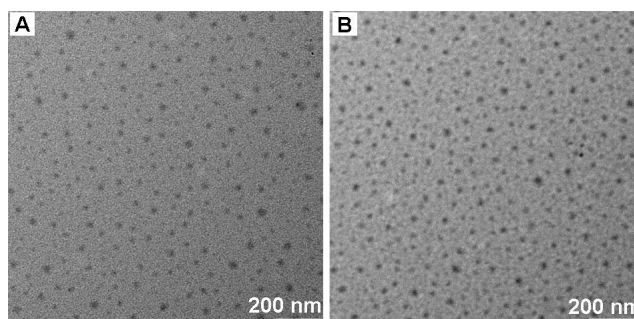


Fig. 2 TEM images of **PhE-MTP-20** NPs (A) and **PhE-MTP-40** NPs (B). Many spherical nanoparticles with diameter at tens of nanometers can be clearly identified by TEM observation, implying the successful formation of **PhE-MTP** NPs in aqueous solution.

The FT-IR spectra of MTP, **PhE-MTP-20** NPs, **PhE-MTP-40** NPs were shown in Fig. 3A. It can be seen that a series of absorption peaks located at 954, 1058, 1254, and 1705 cm^{-1} were observed, indicating that the functional groups such as $-\text{N}(\text{CH}_3)_3$, POCH_2 and $\text{C}=\text{O}$ were existed in MTP. On the other hand, $\text{C}=\text{C}$ stretching vibration located at 1636 cm^{-1} was also observed in MTP.⁶⁵⁻⁶⁷ After formation of **PhE-MTP** NPs, the absorption located at 1058 cm^{-1} can still be observed. However, the intensity located at 1636 cm^{-1} is significantly decreased. These results suggested that MTP was successfully copolymerized with PhE. On the other hand, intensity of absorption peaks at 2977 and 2922 cm^{-1} assigned to alkyl chain of PhE were obviously enhanced, further confirming the successful incorporation of PhE into **PhE-MTP** copolymers. The chemical compositions of MTP, **PhE-MTP-20** NPs and **PhE-MTP-40** NPs were characterized by XPS. As shown in Fig. 3B, the elements including Carbon (C), Nitrogen (N), Oxygen (O), Phosphorus (P) were detected by survey curve of XPS spectra ranged from 0-1200 eV. The existence element P

in samples of **PhE-MTP** NPs further confirming the successful copolymerization of PhE and MTP.

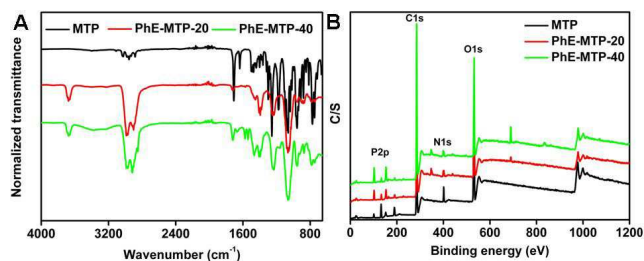


Fig. 3 (A) FT-IR spectra of MTP, **PhE-MTP-20** NPs and **PhE-MTP-40** NPs. The increase of absorbance intensity at 2977 and 2922 cm^{-1} and decrease of absorbance intensity at 1636 cm^{-1} evidenced the successful formation of **PhE-MTP** NPs. (B) Survey curves of XPS spectra of MTP, **PhE-MTP-20** NPs and **PhE-MTP-40** NPs. The existence of Phosphorus in samples of **PhE-MTP** NPs further confirmed the successful formation of **PhE-MTP** NPs.

More detailed information of XPS spectra of C, N, O and P are shown in Fig. 4. It can be seen that binding energy peaks of C1s in MTP are located at 284.4, 285.7 and 288.2 eV, which can be ascribed to C-C, C-O and C-N, respectively. Upon formation of **PhE-MTP** NPs, the signal of binding energy peak located at 284.4 eV was obviously enhanced while intensity of binding energy peaks located at 285.7 and 288.2 eV were significantly decreased (Fig. 4A). On the other hand, the binding energy peak of N1s at 401.1 eV could be ascribed to the C-N of MTP (Fig. 4B). However, in the sample of **PhE-MTP** NPs, another binding energy peak located at 398.0 eV from PhE was emerged, indicating the successful formation of **PhE-MTP** NPs. Furthermore, two binding energy peaks located at 529.0 and 531.0 eV were observed in the sample of MTP (Fig. 4C), which could be assigned to the P-O and C-O, respectively. After formation of **PhE-MTP** NPs, the intensity of P-O was decreased while intensity of C-O was enhanced, further implying successful formation of **PhE-MTP** NPs. Finally, P2p signal was found both in MTP and **PhE-MTP** NPs, giving direct evidence for formation of **PhE-MTP** NPs (Fig. 4D). Based on XPS spectra, the element percentages of C, N, O, P in the samples could be calculated. Results showed that element content of C, N, O, P are 59.48, 4.34, 31.2, 4.98 for MTP (Table S1). As compared with MTP, the percentage of P was obviously decreased in the samples of **PhE-MTP** NPs (1.92 for **PhE-MTP-20** NPs and 1.47 for **PhE-MTP-40** NPs). The increase intensity of C and decrease of P further confirming successful formation of **PhE-MTP** NPs.

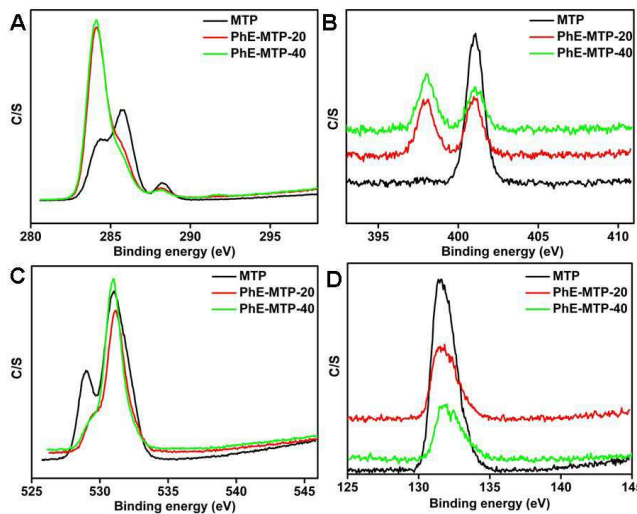


Fig. 4 XPS characterization of MTP, **PhE-MTP-20** NPs and **PhE-MTP-40** NPs. (A) C1s, (B) N1s, (C) O1s and (D) P2p.

Due to the amphiphilic properties, **PhE-MTP** copolymers are prone to self-assemble into spherical nanoparticles in aqueous solution (Fig. 2). The hydrophobic dye (PhE) was encapsulated in the core of **PhE-MTP** NPs while hydrophilic segments (MTP) were expended into water, which made these luminescent polymeric nanoparticles excellent water dispersibility. Even **PhE-MTP** NPs were dispersed in water for more than one week, no obvious precipitation was observed (left cuvette of Fig. 5). On the other hand, due to the aggregation of PhE in the core of nanoparticles, **PhE-MTP** NPs showed strong yellow fluorescence in water (right cuvette of Fig. 5). The optical properties of **PhE-MTP** NPs were further investigated by UV-vis spectroscopy and fluorescence spectroscopy. Two absorption peaks located at 326 and 425 nm were observed by UV-vis spectroscopy (Fig. 5A). These peaks should be ascribed to PhE because MTP showed no absorption peaks in these regions. Fluorescence spectra shown in Fig. 5B suggested that when **PhE-MTP** NPs were excited with 488 nm wavelength, the emission peak of **PhE-MTP** NPs was located at 581 nm. Excitation spectra of **PhE-MTP** NPs was obtained using 581 nm as emission wavelength. It can be seen that two peaks located at 340 and 435 nm were found in excitation spectra. Based on excitation spectra, we found that **PhE-MTP** NPs could be excited by different wavelength ranged from 300-500 nm, the broad excitation characteristics made **PhE-MTP** NPs promising for biological applications. The fluorescence quantum yields of **PhE-MTP-20** NPs and **PhE-MTP-40** NPs in water are 9.84% and 9.21% using Rhodamine 6G in ethanol as the standard. The quantum yields of **PhE-MTP** NPs is much higher than our previous reported AIE dots.⁵⁸ Furthermore, the fluorescence stability of **PhE-MTP** NPs also examined. As shown in Fig. S4, both **PhE-MTP-20** NPs and **PhE-MTP-40** NPs showed excellent photostability after they were irradiated at 488 nm for 30 min. Given the excellent fluorescent properties of **PhE-MTP** NPs, we could expect that **PhE-MTP** NPs are very suitable for bioimaging applications as compared with the small organic dyes.

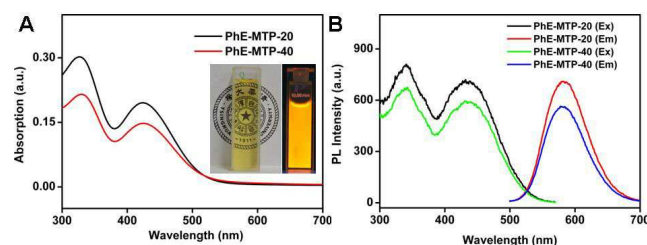


Fig. 5 Spectroscopy characterization of **PhE-MTP** NPs. (A) UV-Vis spectra inset are optical (left cuvette) and fluorescence images (right cuvette) of **PhE-MTP-20** NPs in water; (B) fluorescence spectra of **PhE-MTP** NPs, the excitation wavelength is 488 nm, the emission peaks are located at 581 nm for **PhE-MTP** NPs.

3.2 Biocompatibility of PhE-MTP NPs

Biocompatibility evaluation is a necessary step for biomedical applications of materials.^{68, 69} In this work, optical microscopy observation and cell viability examination were used to evaluate their biocompatibility. **Fig. S5** showed the optical microscopy image of cells incubated with different concentrations (0-120 $\mu\text{g mL}^{-1}$) of **PhE-MTP-20** NPs for 24 h. As compared with the control cells, cells still adhered to cell plate very well when they were incubated with 20, 80 and 120 $\mu\text{g mL}^{-1}$ of **PhE-MTP-20** NPs. No cell number decrease was found by optical microscopy observation. And no significant difference was observed between **PhE-MTP-20** NPs and **PhE-MTP-40** NPs. These results suggested that **PhE-MTP** NPs possessed excellent biocompatibility. CCK-8 assay was further adopted to evaluate the biocompatibility of **PhE-MTP** NPs. Based on CCK-8 results, no cell viability decrease was found when cells were incubated with different concentrations of **PhE-MTP** NPs for 8 and 24 h. The cell viability values still greater than 95% even the concentration of **PhE-MTP** NPs is as high as 120 $\mu\text{g mL}^{-1}$ (**Fig. 6**). These results are well consistent with optical microscopy observation, further confirming good biocompatibility of **PhE-MTP** NPs. Considered the high water dispersibility, remarkable optical properties and excellent biocompatibility of **PhE-MTP** NPs, biological imaging applications of these AIE dye based NPs were subsequently evaluated.

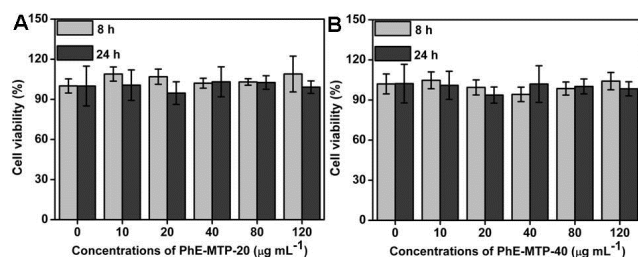


Fig. 6 Cell viability of **PhE-MTP** NPs determined by CCK-8 assay, (A) **PhE-MTP-20** NPs, (B) **PhE-MTP-40** NPs. Cells were incubated with different concentrations (10-120 $\mu\text{g mL}^{-1}$) of **PhE-MTP** NPs for 8 and 24 h.

3.3 Biological images of PhE-MTP NPs

To evaluate their potential biomedical applications, the cellular uptake of **PhE-MTP** NPs was investigated by CLSM.⁷⁰ As shown in **Fig. 7**, the cell uptake of **PhE-MTP** NPs were found in the cell membrane areas, leaving a larger dark area surrounded by yellow fluorescence (**Fig. 7B** and

C). These results are obviously different from many other AIE dye based nanoparticles as described previously, which suggested that AIE dye based nanoparticles were internalized by cells via phagocytosis and mainly distributed in the whole cytoplasm.¹⁹⁻²¹ The significant difference between the **PhE-MTP** NPs and other AIE dye based nanoparticles is likely due to their different physicochemical properties. It is well known that structure of MTP is very similar with the phospholipids of cell membrane. Therefore, after **PhE-MTP** NPs were incubated with cells, they were first merged with cell membrane. At the same time, the AIE dye were therefore encapsulated in cell membrane, which made **PhE-MTP** NPs potential for cell membrane dyeing. On the other hand, due to the flexibility of RAFT polymerization, many other functional monomers could also be introduced into our polymeric system. Thus properties of these luminescent polymeric nanoparticles could be finely tuned by adjusting polymerization parameters. Furthermore, many other functional components such as targeting agents can also be linked onto these polymeric nanoparticles via subsequent coupling reactions. Therefore polymeric nanoparticles with targeting ability could be achieved.

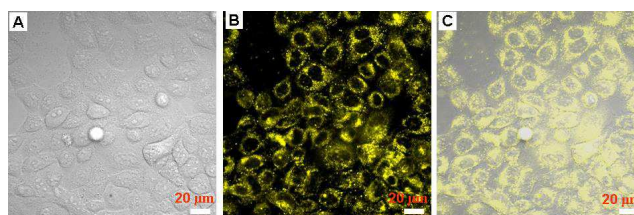


Fig. 7 CLSM images of A549 cells incubated with 10 $\mu\text{g mL}^{-1}$ of **PhE-MTP-20** NPs for 3 h. (A) bright field, (B) excited with 488 nm laser, (C) merge image of A and B. Scale bar = 20 μm .

4. Conclusion

In summary, novel luminescent polymeric nanoparticles based on a polymerizable AIE dye (PhE) and a zwitterionic monomer were prepared via RAFT polymerization. The **PhE-MTP** NPs showed uniform spherical morphology with diameter at tens of nanometers. They can be well dispersed in aqueous solution and emitted strong yellow fluorescence because PhE was aggregated in the core of **PhE-MTP** NPs. These AIE dye based luminescent polymeric nanoparticles showed excellent biocompatibility with A549 cells and mainly distributed in cell membrane after they were incubated with cells. The cell uptake behavior of **PhE-MTP** NPs were significant different from many other AIE dye based nanoparticles, which were mainly internalized into cells through phagocytosis.¹⁹⁻²¹ It is possible ascribed to the difference physicochemical properties of **PhE-MTP** NPs and other AIE dye based nanoparticles. Combination of the remarkable fluorescence, high water dispersibility and excellent biocompatibility, thus AIE dye based zwitterionic luminescent polymeric nanoparticles are expected highly potential for various biomedical applications.

Acknowledgements

This research was supported by the National Science

Foundation of China (no. 21134004, 21201108, 51363016), and the National 973 Project (no. 2011CB935700), China Postdoctoral Science Foundation (no. 2012M520388, 2012M520243, 2013T60100, 2013T60178).

Notes

^a Department of Chemistry/Institute of Polymers, Nanchang University, 999 Xuefu Avenue, Nanchang 330031, China. ^b Department of Chemistry and Key Laboratory of Bioorganic Phosphorus Chemistry & Chemical Biology (Ministry of Education), Tsinghua University, Beijing, 100084, P. R. China. ^c College of Chemistry and Biology, Zhongshan Institute, University of Electronic Science & Technology of China, Zhongshan 528402, China

Xiaoyongzhang1980@gmail.com; weiyen@tsinghua.edu.cn

† Electronic Supplementary Information (ESI) available: [detailed information about ¹H NMR spectra of PhE-MTP NPs, size distribution of PhE-MTP NPs in water, and microscopy observation of cells after they were incubated with different concentrations of PhE-MTP NPs *et al*]. See DOI: 10.1039/b000000x/

References

1. X. Michalet, F. Pinaud, L. Bentolila, J. Tsay, S. Doose, J. Li, G. Sundaresan, A. Wu, S. Gambhir and S. Weiss, *Science*, 2005, **307**, 538-544.
2. R. Weissleder, *Science*, 2006, **312**, 1168-1171.
3. A. Bhirde, J. Xie, M. Swierczewska and X. Chen, *Nanoscale*, 2011, **3**, 142-153.
4. S. Chandra, S. H. Pathan, S. Mitra, B. H. Modha, A. Goswami and P. Pramanik, *RSC Adv.*, 2012, **2**, 3602-3606.
5. B. De and N. Karak, *RSC Adv.*, 2013, **3**, 8286-8290.
6. S. Mitra, S. Chandra, T. Kundu, R. Banerjee, P. Pramanik and A. Goswami, *RSC Adv.*, 2012, **2**, 12129-12131.
7. S. Mitra, S. Chandra, S. H. Pathan, N. Sikdar, P. Pramanik and A. Goswami, *RSC Adv.*, 2013, **3**, 3189-3193.
8. Z. Qian, J. Ma, X. Shan, L. Shao, J. Zhou, J. Chen and H. Feng, *RSC Adv.*, 2013, **3**, 14571-14579.
9. A. Sachdev, I. Matai, S. U. Kumar, B. Bhushan, P. Dubey and P. Gopinath, *RSC Adv.*, 2013, **3**, 16958-16961.
10. X. Zhang, S. Wang, M. Liu, B. Yang, L. Feng, Y. Ji, L. Tao and Y. Wei, *Phys. Chem. Chem. Phys.*, 2013, **15**, 19013-19018.
11. X. Zhang, S. Wang, C. Zhu, M. Liu, Y. Ji, L. Feng, L. Tao and Y. Wei, *J. Colloid Interface Sci.*, 2013, **397**, 39-44.
12. J. Hui, X. Zhang, Z. Zhang, S. Wang, L. Tao, Y. Wei and X. Wang, *Nanoscale*, 2012, **4**, 6967-6970.
13. X. Zhang, J. Hui, B. Yang, Y. Yang, D. Fan, M. Liu, L. Tao and Y. Wei, *Polym. Chem.*, 2013, **4**, 4120-4125.
14. H. S. Choi, W. Liu, P. Misra, E. Tanaka, J. P. Zimmer, B. I. Ipe, M. G. Bawendi and J. V. Frangioni, *Nat. Biotechnol.*, 2007, **25**, 1165-1170.
15. S. Liu, H. Zhang, Y. Qiao and X. Su, *RSC Adv.*, 2012, **2**, 819-825.
16. X. Zhang, X. Zhang, B. Yang, J. Hui, M. Liu, Z. Chi, S. Liu, J. Xu and Y. Wei, *Polym. Chem.*, 2014, **5**, 318-322.
17. X. Zhang, X. Zhang, B. Yang, J. Hui, M. Liu, Z. Chi, S. Liu, J. Xu and Y. Wei, *Polym. Chem.*, 2014, **5**, 683-688.
18. X. Zhang, X. Zhang, B. Yang, J. Hui, M. Liu, W. Liu, Y. Chen and Y. Wei, *Polym. Chem.*, 2014, **5**, 689-693.
19. X. Zhang, X. Zhang, B. Yang, M. Liu, W. Liu, Y. Chen and Y. Wei, *Polym. Chem.*, 2013, **4**, 4317-4321.
20. X. Zhang, X. Zhang, B. Yang, M. Liu, W. Liu, Y. Chen and Y. Wei, *Polym. Chem.*, 2014, **5**, 356-360.
21. X. Zhang, X. Zhang, B. Yang, M. Liu, W. Liu, Y. Chen and Y. Wei, *Polym. Chem.*, 2014, **5**, 399-404.
22. J. Liu, D. Ding, J. Geng and B. Liu, *Polym. Chem.*, 2012, **3**, 1567-1575.
23. R. Zhan, A. J. H. Tan and B. Liu, *Polym. Chem.*, 2011, **2**, 417-421.
24. P. Zhang, J. Chen, F. Huang, Z. Zeng, J. Hu, P. Yi, F. Zeng and S. Wu, *Polym. Chem.*, 2013, **4**, 2325-2332.
25. X. Zhang, M. Liu, B. Yang, X. Zhang, Z. Chi, S. Liu, J. Xu and Y. Wei, *Polym. Chem.*, 2013, **4**, 5060-5064.
26. M. Liu, X. Zhang, B. Yang, F. Deng, J. Ji, Y. Yang, Z. Huang, Z. Xiaoyong and W. Yen, *RSC Adv.*, 2014, **4**, 22294-22298.
27. K. Li and B. Liu, *Chem. Soc. Rev.*, 2014, 10.1039/C1034CS00014E.
28. X. Zhang, X. Zhang, L. tao, Z. Chi, J. Xu and Y. Wei, *J. Mater. Chem. B*, 2014, 10.1039/C1034TB00291A.
29. L. Feng, C. Zhu, H. Yuan, L. Liu, F. Lv and S. Wang, *Chem. Soc. Rev.*, 2013, **42**, 6620-6633.
30. Y. Hong, J. W. Y. Lam and B. Z. Tang, *Chem. Soc. Rev.*, 2011, **40**, 5361-5388.
31. Q. Zhao, C. Huang and F. Li, *Chem. Soc. Rev.*, 2011, **40**, 2508-2524.
32. X. Feng, L. Liu, S. Wang and D. Zhu, *Chem. Soc. Rev.*, 2010, **39**, 2411-2419.
33. X. Zhang, X. Zhang, S. Wang, M. Liu, Y. Zhang, L. Tao and Y. Wei, *ACS Appl. Mater. Interfaces*, 2013, **5**, 1943-1947.
34. V. Ibrahimova, S. Ekiz, Ö. Gezici and D. Tuncel, *Polym. Chem.*, 2012, **2**, 2818-2824.
35. H. Lu, X. Zhao, W. Tian, Q. Wang and J. Shi, *RSC Adv.*, 2014, **4**, 18460-18466.
36. Z. Wang, S. Chen, J. W. Lam, W. Qin, R. T. Kwok, N. Xie, Q. Hu and B. Z. Tang, *J. Am. Chem. Soc.*, 2013, **135**, 8238-8245.
37. J. Luo, Z. Xie, J. W. Y. Lam, L. Cheng, H. Chen, C. Qiu, H. S. Kwok, X. Zhan, Y. Liu, D. Zhu and B. Z. Tang, *Chem. Commun.*, 2001, **37**, 1740-1741.
38. Y. Hong, J. W. Lam and B. Z. Tang, *Chem. Commun.*, 2009, **45**, 4332-4353.
39. Y. Liu, X. Feng, J.-g. Zhi and B. Tong, *Chin. J. Polym. Sci.*, 2012, **30**, 443-450.
40. D. Chen, X. Feng, S. Gu, B. Tong, J. Shi, J. Zhi and Y. Dong, *Chinese Sci. Bull.*, 2013, **58**, 2728-2732.
41. X. Zhang, Z. Chi, B. Xu, C. Chen, X. Zhou, Y. Zhang, S. Liu and J. Xu, *J. Mater. Chem.*, 2012, **22**, 18505-18513.
42. X. Zhang, Z. Chi, J. Zhang, H. Li, B. Xu, X. Li, S. Liu, Y. Zhang and J. Xu, *J. Phys. Chem. B*, 2011, **115**, 7606-7611.
43. X. Zhang, Z. Chi, H. Li, B. Xu, X. Li, W. Zhou, S. Liu, Y. Zhang and J. Xu, *Chem.-Asian J.*, 2011, **6**, 808-811.
44. A. Qin, J. W. Lam and B. Z. Tang, *Prog. Polym. Sci.*, 2012, **37**, 182-209.
45. D. Ding, C. C. Goh, G. Feng, Z. Zhao, J. Liu, R. Liu, N. Tomczak, J. Geng, B. Z. Tang and L. G. Ng, *Adv. Mater.*, 2013, **25**, 6083-6088.
46. J. Kim, J. E. Lee, S. H. Lee, J. H. Yu, J. H. Lee, T. G. Park and T. Hyeon, *Adv. Mater.*, 2008, **20**, 478-483.
47. D. Li, Z. Liang, J. Chen, J. Yu and R. Xu, *Dalton Trans.*, 2013, **42**, 9877-9833.
48. H. Wu, T. Yang, Q. Zhao, J. Zhou, C. Li and F. Li, *Dalton Trans.*, 2011, **40**, 1969-1976.
49. H. Shi, R. T. Kwok, J. Liu, B. Xing, B. Z. Tang and B. Liu, *J. Am. Chem. Soc.*, 2012, **134**, 17972-17981.
50. H. Shi, J. Liu, J. Geng, B. Z. Tang and B. Liu, *J. Am. Chem. Soc.*, 2012, **134**, 9569-9572.
51. C. Ma, Q. Ling, S. Xu, H. Zhu, G. Zhang, X. Zhou, Z. Chi, S. Liu, Y. Zhang and J. Xu, *Macromol. Biosci.*, 2014, **14**, 235-243.
52. M. Li, Y. Hong, Z. Wang, S. Chen, M. Gao, R. T. Kwok, W. Qin, J. W. Lam, Q. Zheng and B. Z. Tang, *Macromol. Rapid Commun.*, 2013, **34**, 767-771.
53. X. Zhang, X. Zhang, B. Yang, L. Liu, J. Hui, M. Liu, Y. Chen and Y. Wei, *RSC Adv.*, 2014, **4**, 10060-10066.
54. X. Zhang, X. Zhang, B. Yang, S. Wang, M. Liu, Y. Zhang and L. Tao, *RSC Adv.*, 2013, **3**, 9633-9636.
55. X. Zhang, X. Zhang, B. Yang, J. Hui, M. Liu, Z. Chi, S. Liu and J. Xu, *J. Mater. Chem. C*, 2014, **2**, 816-820.
56. R. Hu, N. L. Leung and B. Z. Tang, *Chem. Soc. Rev.*, 2014, 10.1039/C1034CS00044G.
57. A. B. Lowe and C. L. McCormick, *Chem. Rev.*, 2002, **102**, 4177-4190.
58. X. Zhang, X. Zhang, B. Yang, M. Liu and Y. Wei, *Colloids Surf. B Biointerfaces*, 2014, **116**, 739-744.
59. H. Qi, M. Liu, L. Xu, L. Feng, I. Tao, Y. Ji, X. Zhang and Y. Wei, *Toxicol. Res.*, 2013, **2**, 427-433.

-
60. X. Zhang, W. Hu, J. Li, L. Tao and Y. Wei, *Toxicol. Res.*, 2012, **1**, 62-68.
 61. X. Zhang, H. Qi, S. Wang, L. Feng, Y. Ji, L. Tao, S. Li and Y. Wei, *Toxicol. Res.*, 2012, **1**, 201-205.
 - 5 62. X. Zhang, S. Wang, M. Liu, J. Hui, B. Yang, L. Tao and Y. Wei, *Toxicol. Res.*, 2013, **2**, 335-346.
 63. X. Zhang, X. Zhang, B. Yang, Y. Zhang, M. Liu, W. Liu, Y. Chen and Y. Wei, *Colloids Surf. B Biointerfaces*, 2014, **1**, 435-441.
 64. X. Zhang, M. Liu, B. Yang, X. Zhang and Y. Wei, *Colloids Surf. B Biointerfaces*, 2013, **112**, 81-86.
 - 10 65. X. Zhang, J. Ji, X. Zhang, B. Yang, M. Liu, W. Liu, L. Tao, Y. Chen and Y. Wei, *RSC Adv.*, 2013, **3**, 21817-21823.
 66. X. Zhang, M. Liu, Y. Zhang, B. Yang, Y. Ji, L. Feng, L. Tao, S. Li and Y. Wei, *RSC Adv.*, 2012, **2**, 12153-12155.
 - 15 67. X. Zhang, C. Fu, L. Feng, Y. Ji, L. Tao, Q. Huang, S. Li and Y. Wei, *Polymer*, 2012, **53**, 3178-3184.
 68. L. Xu, X. Zhang, C. Zhu, Y. Zhang, C. Fu, B. Yang, L. Tao and Y. Wei, *J. Biomater. Sci-Polym E*, 2013, **24**, 1564-1574.
 69. X. Zhang, S. Wang, C. Fu, L. Feng, Y. Ji, L. Tao, S. Li and Y. Wei, *Polym. Chem.*, 2012, **3**, 2716-2719.
 - 20 70. B. Yang, Y. Zhang, X. Zhang, L. Tao, S. Li and Y. Wei, *Polym. Chem.*, 2012, **3**, 3235-3238.